ELSEVIER

Sensors and Actuators B 81 (2002) 377–383

SENSORS AND ACTUATORS B CHEMICAL

www.elsevier.com/locate/sensorb

The design of an in-plane compliance structure for microfluidical systems

T.T. Veenstra[a,*], N.R. Sharma[b], F.K. Forster[b], J.G.E. Gardeniers[c], M.C. Elwenspoek[a], A. van den Berg[a]

[a]*MESA Research Institute, Transducers Science and Technology Group, University of Twente, P.O. Box 217, 7500 AE Enschede, The Netherlands*
[b]*Mechanical Engineering Department, University of Washington, Campus Box 352600, Seattle, WA 98195-2600, USA*
[c]*Micronit Microfluidics BV Hengelosestraat 705, 7521 PA Enschede, The Netherlands*

Accepted 21 September 2001

Abstract

Two compliance structures for the use in liquid-based microfluidic systems have been realized with the aid of silicon micromachining. The basic principle is that these structures contain air bubbles that dampen the flow and pressure variations that may arise from a micropump. The compliance structures were specifically designed to work with the no moving parts valve (NMPV) pump [Proc. ASME Fluids Eng. Division, 1995, in press]. The structures were modeled and simulated. From the results of these simulations and the model, design rules for the compliance are formulated.

Measurements on the compliance structures could only be performed for the steady state. These measurements were in very good agreement with the model. Working with two sets of pumps showed that pumps without the compliance structure needed an external compliance in order to get them to work, whereas the pumps with the on-chip compliance pumped right away.

Keywords: Microfluidics; Compliance; Pumps; Micropumps; Liquid

1. Introduction

Since in microfluidics most pumps are membrane pumps, the flow resulting from micropumps [1] will be pulsed in some sort of way [2–7]. Problems arising from this pulsed flow are summarized in [8]. For a micropump with check-valves, the flow will look more or less like a rectified sine. A pump with hydrodynamic valves (as the pump, no moving parts valve pump, NMPV) produces a sinusoidal flow with an offset, resulting in a net flow. The variations around this net flow are easily five times as large as the net flow itself. If there would be no compliance in the fluidic system, the flow variations would have to be present throughout the whole system, i.e. the whole column of fluid would have to be displaced. This would require a very strong membrane actuation and would very probably result in cavitation of the pumpchamber. The incorporation of an additional compliance directly before and after the micropump can solve this problem. The flow variations are taken up by the compliance, whereas the net flow can go into the main fluidical system. Up to now, a macrocompliance was used to get the NMPV pump working (Fig. 1).

In this paper, we present a micromachined compliance, which consists of an air bubble trapped in a side branch of the main liquid transport channel.

2. Basic design

The actual compliance is formed with trapped air. The basic idea is that the compressible air bubble will dampen pressure pulses in the liquid stream. We designed two types of air traps. Both designs are shown in Fig. 2. The first layout is designed to trap air bubbles in the far ends of the numerous narrow channels. The second layout consists of one large chamber next to the main channel.

Both structures were filled partly due to the surface tension which brings the fluid into the chamber or side-channel. This causes the pressure of the air in the structure to rise slightly. A pressure fluctuation in the main channel causes fluid to flow in (and out) the side structure. The fact,

* Corresponding author.

0925-4005/02/$ – see front matter
PII: S0925-4005(01)00964-9

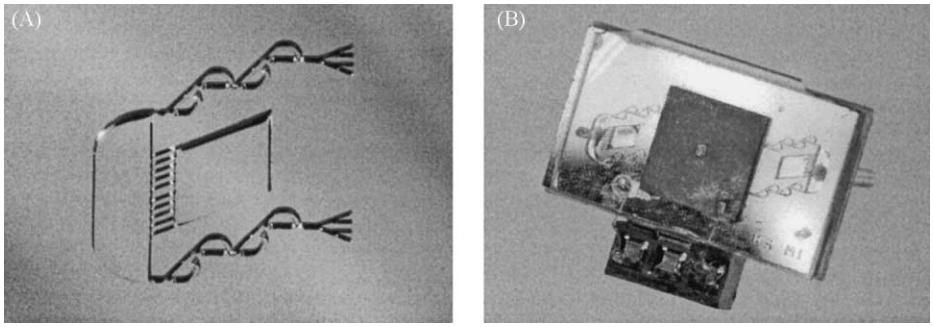

Fig. 1. Photographs of completed devices: (A) the compliance structure in between the outlet valves of a NMPV pump; (B) a completed NMPV micropump with integrated compliance structure.

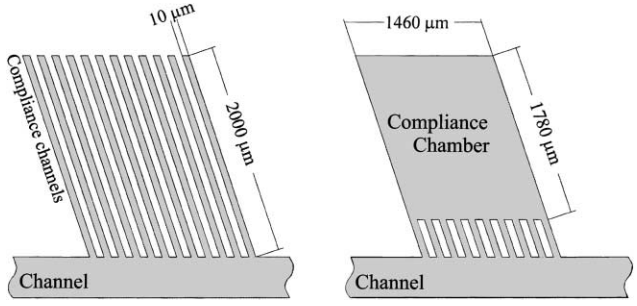

Fig. 2. The layout of the realized samples. The first layout consists of parallel channels, the other of a single chamber with multiple inlets.

that due to the surface tension some fluid is stored in the side-channel makes both positive and negative flow variations possible.

For large flows into the compliance, the compliance does not act linearly. Since the air pressure will be raised due to the incoming fluid, the effort that is needed to get fluid into the compliance will increase.

3. Modeling

The static and dynamic behavior of the compliance structures are modeled. From the full equation of motion, a steady state solution is derived. After this, the dynamic response of the system is calculated from the linearized system. For the compliance structure with the large chamber, a complete solution as for the little side-channel was not found. This is due to the fact, that the shape of the meniscus in the chamber cannot be predicted accurately.

For modeling, the behavior of the side-channel, the fluid in the side-channel was considered as a mass (fluid in the side-channel) attached to a spring (trapped air) and a damper (fluid resistance of the filled part of the side-channel). The surface tension at the air–water interface introduces an offset for the mass-spring-damper system.

The model describes the position of the air–water surface as function of all other parameters of the system (Fig. 3). The force balance is as follows:

$$M\ddot{x} = P_{\text{fluid}} wd + 2\gamma_s (w + d)\cos\alpha - p_{\text{air}} wd - w^2 d^2 R_{\text{ch}} \dot{x} \tag{1}$$

where x is the position of the surface, M the mass of the fluid in the side-channel, P_{fluid} and P_{air} the pressure at the inlet of the side-channel and the pressure of the trapped air, respectively, w and d the width and depth of the side-channel, γ_s and α the surface tension and the contact angle of an air–water–glass interface and R_{ch}, the fluid resistance of the filled part of the side-channel.

Mass, resistance and trapped air pressure, all depend on the position of the surface. The incorporated mass is

$$M = \rho_{H_2O} dwx \tag{2}$$

where ρ_{H_2O} is the density of water.

The pressure of the trapped air depends on the frequency of the volume variations. For slow variations, there will be enough time to exchange heat between the gas and its surroundings. Therefore, the isothermal approach is used for slow variations (Eq. (3)). However, for variations with a frequency in the order of magnitude of the operating frequency of the NMPV pump (∼3 kHz), the gas will not reach an equilibrium state. For these fast variations, the process is considered adiabatic (Eq. (4)). This was verified for a 10-μm wide channel. After a sudden temperature change of the gas,

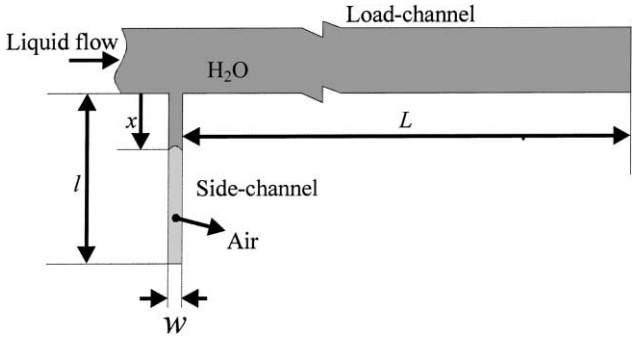

Fig. 3. The basic layout of the compliance structure.

it takes approximately 200 μs to transport enough heat to (or from) the gas to keep the temperature of the gas at ambient temperature.

$$P_{\text{air}} = P_0\left(\frac{l}{l-x}\right) \qquad \text{(isothermal)} \tag{3}$$

$$P_{\text{air}} = P_0\left(\frac{l}{l-x}\right)^{\gamma} \qquad \text{(adiabatic)} \tag{4}$$

where P_0 is the initial pressure before compression, l the length of the side-channel and γ the specific heat ratio for the trapped gas ($\gamma = 1.4$ for air). Both expressions were used, since the filling of the channel will be a slow process (there is enough time to exchange heat with the surroundings), so the isothermal law applies, whereas the actual flow variations will be fast variations (≈3 kHz for the NMPV pump) raising the need for the adiabatic equation. The final pressure from the isothermal equation will be the initial pressure for the adiabatic equation.

The fluid resistance of the filled part of the side-channel varies with the length of this filled part, x. However, care has to be taken which model is applied. If the channel width is much smaller than its depth, then the channel can be treated as a slit, but in case of depth and width being of the same order of magnitude, the fluid resistance should be considered as the resistance from a rectangular channel [9,10]

$$R_{\text{fluid}} = \frac{3\mu_{\text{H}_2\text{O}}x}{w^3 d} \qquad (\text{slit}, d \gg w) \tag{5}$$

$$R_{\text{fluid}} = \frac{128\mu_{\text{H}_2\text{O}}x}{\pi D_{\text{eff}}^4} \qquad (\text{rectangular}, d = \text{O}(w)) \tag{6}$$

This effective diameter is given by

$$D_{\text{eff}} \equiv \frac{4A}{P} = \frac{2wd}{w+d} \tag{7}$$

where A is the cross-sectional area of the channel, and P the wetted perimeter of the channel.

For the steady state, Eq. (1) reduces to

$$0 = p_{\text{fluid}}wd + 2\gamma_{\text{s}}(w+d)\cos\alpha - P_{\text{air}}wd \tag{8}$$

where P_{fluid} is the average pressure in the fluid at the inlet of the side-channel (pressure drop over the load-channel plus atmospheric pressure). From Eqs. (3) and (8), the initial wick-in distance $\hat{x}$ (i.e. the distance the fluid enters the side-channel is easily derived),

$$\hat{x} = l - \frac{lP_0}{P_{\text{fluid}} + 2\gamma_{\text{s}}(w+d)/wd\cos\alpha} \tag{9}$$

The dynamic behavior of this system cannot be solved analytically, unless the non-linearities are removed. The result of linearization about the equilibrium point will be a transfer function $H(\text{j}\omega)$, which will only be valid for small pressure variations

$$\overline{H}(\text{j}\omega) = \frac{\overline{x}(\text{j}\omega)}{\overline{P}(\text{j}\omega)} = k\frac{1}{1 + 2\text{j}\beta(\omega/\omega_0) - (\omega^2/\omega_0^2)} \tag{10}$$

where k is the amplification factor, β the damping constant, ω the applied frequency and ω_0 the natural frequency of the system. Rewriting Eq. (1) into the above form and filling out linearized equations for the mass, the air pressure and the fluid resistance in the side-channel, the natural frequency ω_0 is found to be

$$\omega_0 = \frac{1}{l-\hat{x}}\sqrt{\frac{\gamma l P_{\text{atm}}}{\rho_{\text{H}_2\text{O}}\hat{x}}} \tag{11}$$

in which P_{atm} is the atmospheric pressure.

Integration of Eq. (10), and multiplying by the side-channels cross-sectional area (wd), Eq. (10) results in the side-channels admittance. The admittance of the load-channel is given by

$$\overline{A}_{\text{load}} = \frac{\overline{Q}}{\overline{P}} = \frac{1}{R + \text{j}\omega I} \tag{12}$$

where R is the steady flow resistance of the channel and I the inertance of the fluid in the channel.

The admittance ratio of the side-channel and the load-channel will now determine the magnitude of flow variations in the load-channel due to the pressure variations at the inlet of the load-channel. Fig. 4 shows how the damping of flow variations can be derived from the admittances of the load-channel and the side-channel. The higher corner frequency results from the corner frequency of the side-channel. The

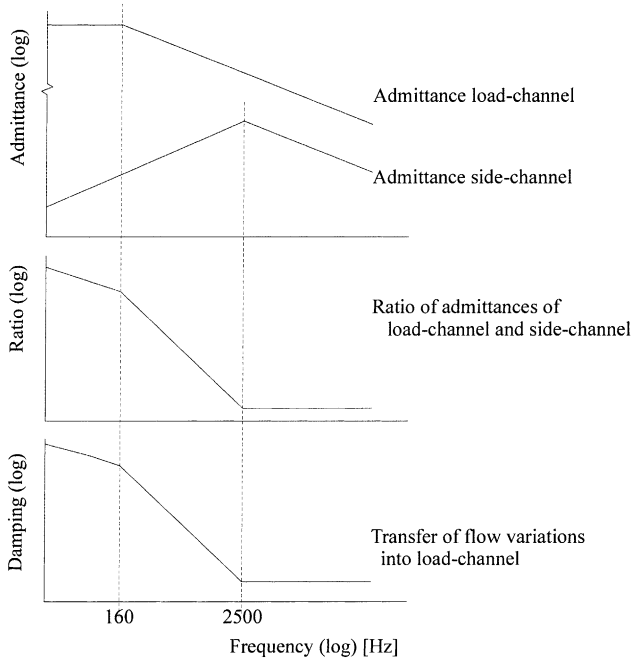

Fig. 4. Construction principle of the damping of flow variations from the admittances of the load- and side-channel.

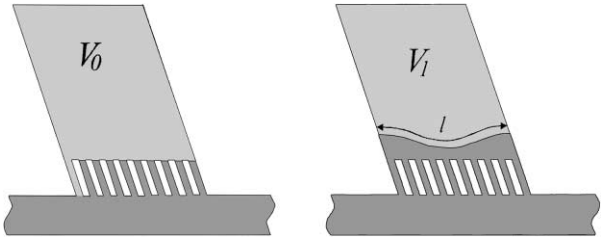

Fig. 5. Meaning of V_0 and l for the chamber compliance structure.

lower corner frequency is at the point where the admittance of both side- and load-channel are the same. For the calculation of the behavior, the following parameters were used for the dimensions of the side-channel and load-channel: $d \times w \times l = 370\,\mu\text{m} \times 10\,\mu\text{m} \times 2000\,\mu\text{m}$ and $0.2\,\text{mm} \times 0.2\,\text{mm} \times 100\,\text{mm}$. The mean flow was 5 μl/s. For this system, the corner frequency of the side-channel is 2500 Hz. The corner frequency of the load-channel is 160 Hz.

Eq. (1) cannot be solved for the chamber compliance structure (Fig. 2), since the shape of the meniscus that will be formed in the chamber cannot be predicted accurately. Therefore, the force of the surface tension dragging fluid into the chamber cannot be predicted. Steady-state measurements can be performed in which the pressure in the chamber as well as the length of the meniscus along the walls of the chamber can be measured. For these conditions, a modified Eq. (8) still holds (see also Fig. 5):

$$P_{\text{atm}} \frac{V_0}{V_1} ld = P_{\text{fluid}} ld + 2\gamma_s (l + d) \cos\alpha \tag{13}$$

where l is the length of the meniscus (as seen from above), d the depth of the chamber and V_0 and V_1 the initial and real volume of the air in the chamber.

4. Simulation

The compliance system was simulated using the simulation package Simulink [11]. The simulated system consisted of a load-channel ($d \times w \times l = 0.2\,\text{mm} \times 0.2\,\text{mm} \times 100\,\text{mm}$) with 40 side-channels ($d \times w \times l = 370\,\mu\text{m} \times 10\,\mu\text{m} \times 2000\,\mu\text{m}$). The flow that was specified at the inlet was a net flow of 5 μl/s with a superimposed sinusoidal flow variation of 0.01 μl/s. These flow variations were kept this much small to ensure that the system would be in its linear region. The flow variations at the output were calculated for different frequencies.

The results from these simulations are shown in Fig. 6. These results closely match the frequency behavior as predicted in Fig. 4.

5. Realization

Samples were prepared using deep reactive ion etching (DRIE) to create the channels and chambers in silicon. The channels were covered by anodic bonding of pyrex to the silicon. Since the exact geometry and surface roughness of the through holes for the fluidical connections are not critical in any way, these through holes were created by drilling, using a diamond drill. See Fig. 7 for the principle of the fabrication process.

Two types of samples were realized. The first type consists of a series of parallel side-channels, whereas the second type is a chamber next to the main channel with 10 parallel inlets into the chamber (see Fig. 2). The channels and chamber are slightly sloped with respect to the main channel in order to fit in between the in/outlet valves of the micropump (see also Fig. 1). The chambers were 1460 μm wide

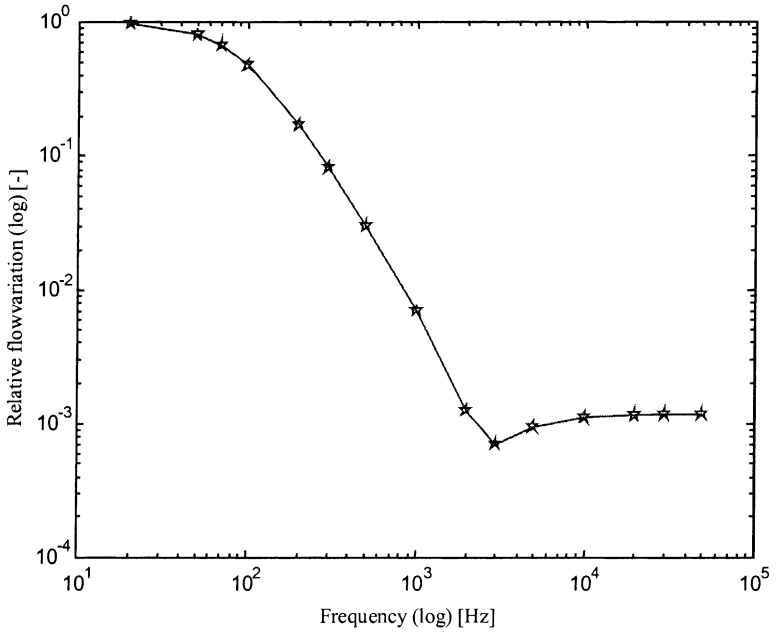

Fig. 6. Frequency dependence of the flow variations in the load-channels respective to the imposed flow variations on the whole system.

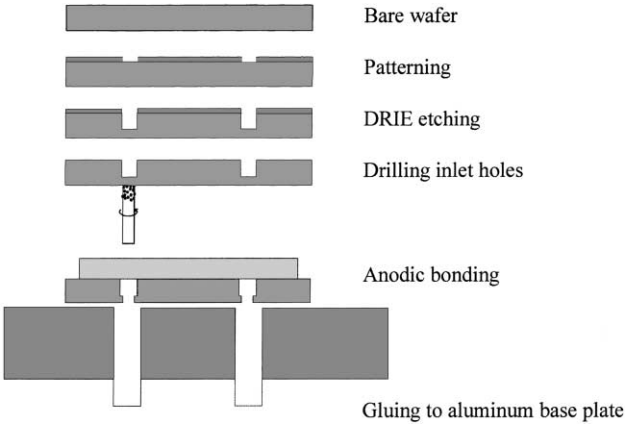

Fig. 7. The fabrication process of the samples.

and 1780 μm long. The side-channels were 10 μm wide and 2000 μm long. There were 384 side-channels on one sample. All etched structures were 373 μm deep.

6. Measurements

A measurement setup has been realized for the characterization of the compliance structure. The setup is schematically shown in Fig. 8. A video camera is used to monitor the sample through a microscope. With this monitor, the position of the meniscus is measured. The system is pressurized with a syringe pump (1 ml B-D syringe on a KD-scientific syringe pump). The pressure in the system is read through a pressure sensor (Entran EPI-411, 3.5 bar range).

The position of the meniscus was read through the microscope. From the so-acquired data, the total volume of air and length of the meniscus can be calculated.

Due to the narrow but deep channel dimensions, the channel did not allow visualization of the meniscus. Therefore, it was not possible for us to obtain information on the position of the meniscus in the small channels. The dimensions of the compliance chamber elements, however, are such that the meniscus can easily be seen. Due to the multiple inlets into these chambers, the chambers first partly filled with water pushed air out of the chamber (Fig. 9). Static measurements on this compliance could, however, still be performed. Starting with the reduced initial volume, the static pressure in the system was gradually increased, which caused the air to be compressed. The compression ratio of the air (initial gas volume over actual gas volume) and the corresponding fluid pressure (measured from the pressure transducer), air pressure (calculated from the measured air volume) and the theoretical pressure due to the surface tension (from the measured length of the meniscus) are shown in Fig. 10. The accuracy of the measurements on the air volume and the length of the meniscus were about 5%.

Also, measurements were performed on the comparison of a pump with the compliance structure and the same pump design without compliance structure. The results are depicted in Fig. 11. The point where the lines stop indicate the point at which the pumps started cavitating. Cavitation is an indication of the fact that the fluid that is coupled to the membrane is too slow to follow the movements of the membrane. The compliance is used to decouple the fluid in the system from the pump membrane. From the figure it is clearly seen that the pump with the compliance structure can reach higher membrane velocities and therefore higher flow

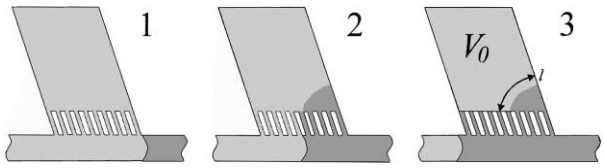

Fig. 9. The way the sample filled, the initial volume V_0 was smaller than meant to be, l denotes the length of the meniscus in the chamber.

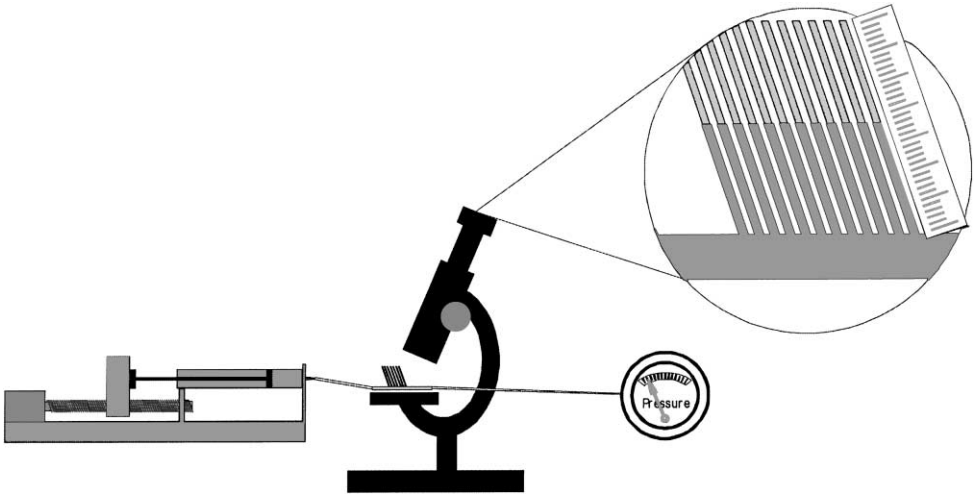

Fig. 8. Schematic of the measurement setup. A microscope is used for the detection of the position of the membrane, a motor driven syringe pump for filling up the system and pressurizing it and a pressure sensor to monitor the actual pressure in the system.

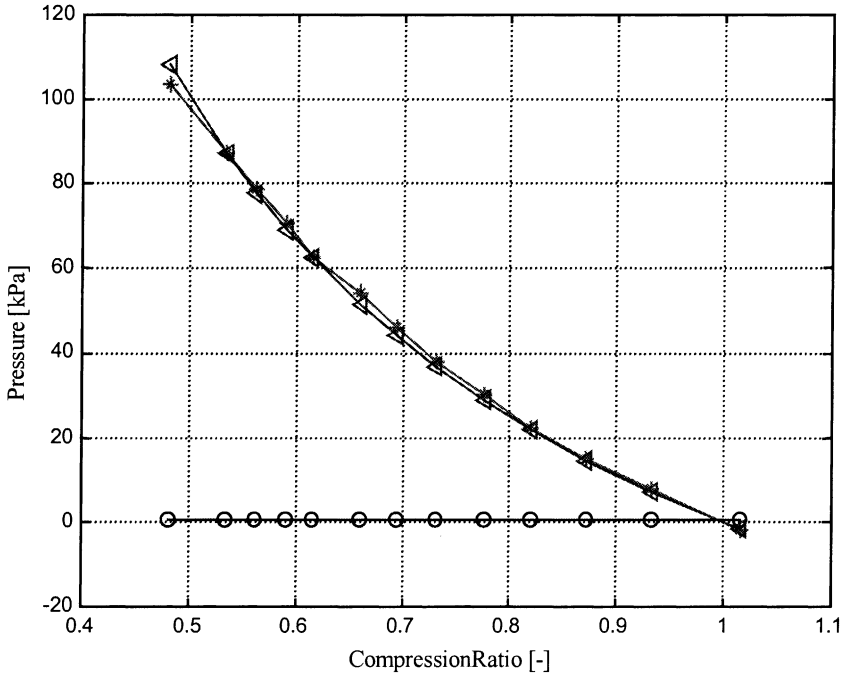

Fig. 10. The pressure in the fluid (∗), results in compression of the air in the compliance chamber. The volume change of the air corresponds to a pressure change of the air (◁). The pressure in the air due to the surface tension is also indicated (○).

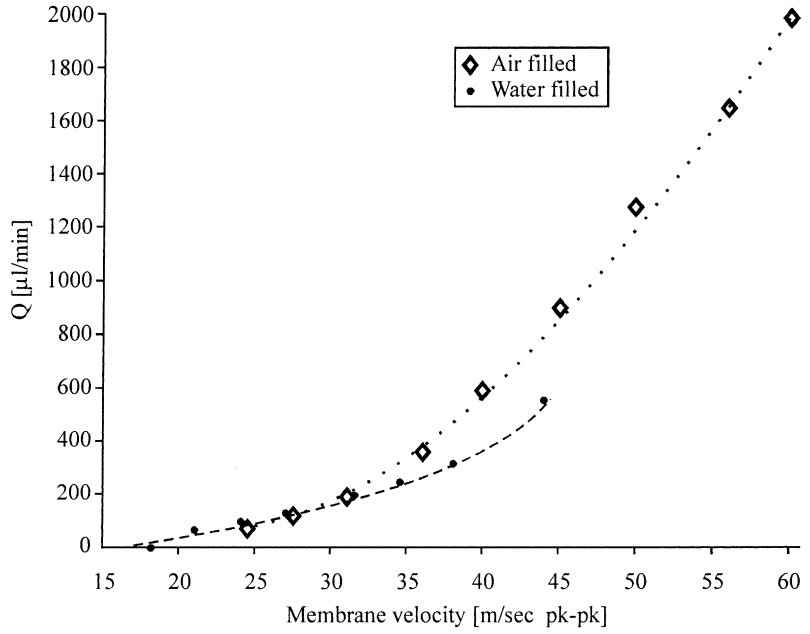

Fig. 11. Measurement results for a pump with (· · ·) and without compliance structure (- - -).

rates as the pump without the compliance. The decoupling works well and therefore it can be concluded that the compliance structure works.

7. Conclusions and future work

A compliance for microfluidical systems has been designed to dampen flow variations resulting from the NMPV pump. This micromachined compliance was used to replace a macro-world compliance which was required for good pump performance. Around the operating frequency of 3 kHz, a theoretical damping of the flow variations of 30 dB was established.

The proof of the working principle has been found in two ways. First, static measurements have been performed on the chamber compliance structure. It is seen, that a raise of the pressure in the system results in the compliance taking in

fluid. The amount of fluid that is absorbed by the compliance matches theory perfectly. Second, two versions of the NMPV pump have been compared. The first version had no compliance structure, whereas the second had the designed compliance connected to its in and outlet. From the comparison it was seen, that the compliance structure enables the pump to deliver almost four times as much fluid per unit time.

The current design of the chamber compliance with its multiple inlets (originally designed for lower resistance) can be improved by reducing the number of inlets to just one. This will prevent the filling of (part of) the chamber with fluid. Any amount of unwanted fluid in the chamber reduces the volume of trapped air and with that the effective compliance.

Acknowledgements

The research was funded by (Dutch Technology Foundation, STW Project TEL 3467) and DARPA (Contracts N660001-97-C-8632 and F30602-98-2-0151). Brian Williams is thanked for his help on the measurements.

References

[1] F.K. Forster, R.L. Bardell, M.A. Afromowitz, N.R. Sharma, A. Blanchard, Design, fabrication and testing of fixed-valve micro pumps, in: proceedings of the ASME Fluidics Eng. Division, Vol 234, pp. 39–44, SAN Francisco, USA, November 1995.
[2] Orlando, USA, January 1999, 17–21.
[3] R. Zengerle, M. Richter, Simulation of microfluid systems, J. Micromech. Microeng. 4 (1994) 192.
[4] SAN Diego, USA, February 1996, 11–15.
[5] J. Ulrich, R. Zengerle, Static and dynamic flow simulation of a KOH etched microvalve using the finite-element method, Sens. Actuators A 53 (1996) 379–385.
[6] M.C. Acero, J.A. Plaza, J. Esteve, M. Carmona, S. Marco, J. Samitier, Design of a modular micropump based on anodic bonding, J. Micromech. Microeng. 7 (1997) 179–182.
[7] T. Bourouina, A. Bosseboeuf, J.P. Grandchamp, Design and simulation of an electrostatic micropump for drug delivery applications, J. Micromech. Microeng. 7 (1997) 186–188.
[8] J.P. Krog, H. Dirac, B. Fabius, P. Gravesen, Requirements of Pumps Used in MicroTAS, microTAS' 98, Banff, 1998.
[9] Shih-I. Pai, Modern Fluid Mechanics, 1st Edition, Science Press, Beijing, 1981 (Chapter II-2).
[10] F.M. White, Fluid Mechanics, Mc Graw-Hill, New York, 1986.
[11] Simulink, The Mathworks Inc., Natick, MA, USA.